Local structural orders in nanostructured Al_2O_3 prepared by high-energy ball milling

2002 J. Phys.: Condens. Matter 14 2101

(http://iopscience.iop.org/0953-8984/14/8/335)

INSTITUTE OF PHYSICS PUBLISHING JOURNAL OF PHYSICS: CONDENSED MATTER

J. Phys.: Condens. Matter **14** (2002) 2101–2117 PII: S0953-8984(02)27287-2

Local structural orders in nanostructured Al_2O_3 prepared by high-energy ball milling

G Scholz[1], R Stösser[1], J Klein[1], G Silly[2], J Y Buzaré[2], Y Laligant[3] and B Ziemer[1]

[1] Institut für Chemie, Humboldt-Universität zu Berlin, Brook-Taylor-Srasse 2, 12489, Berlin, Germany
[2] Laboratoire de Physique de l'Etat Condensé, UMR CNRS n° 6087, France
[3] Laboratoire des Fluorures, UMR CNRS n° 6010, Université du Maine, Avenue Olivier Messiaen, 72085 Le Mans, Cedex 9, France

E-mail: Gudrun.Scholz@rz.hu-berlin.de

Received 27 July 2001, in final form 30 November 2001
Published 15 February 2002
Online at stacks.iop.org/JPhysCM/14/2101

Abstract

Nanostructured Al_2O_3 powders were prepared by high-energy ball milling of corundum. Both the solid state nuclear magnetic resonance spectra of the Al^{3+} ions and the solid state electron paramagnetic resonance spectra of incorporated Fe^{3+} ions are governed by noticeable spectral changes dependent on the duration of the mechanical treatment. The quadrupolar parameters of the ^{27}Al nuclei and the zero-field splitting parameters of the Fe^{3+} ions as well as their statistical distributions were determined as functions of the milling time. Structural changes of the Al_2O_3 matrix were also followed by powder x-ray diffraction and transmission electron microscopy measurements. Direct relations between the structural disorder as obtained by x-ray data and the spin Hamiltonian parameters of both ions could be established.

These results suggest that the milled powders consist of nanocrystalline grains embedded in amorphous grain boundaries even for the longest milling time. The grains can be described in terms of ordered AlO_6-octahedra as in the starting crystalline material exhibiting a slight rhombic distortion. The grain boundaries look like random arrangements of these octahedral units. The specific behaviour of the environment of the Fe^{3+} paramagnetic probe points out that such a point defect acts as an activation centre of the amorphization process.

1. Introduction

The examination of nanostructured powders prepared by the high-energy ball milling route, the determination of their physical and chemical properties are one of the challenges of modern materials science and physics of condensed matter due to their potential applications (new alloys and ceramics, catalysts, high diffusivity materials). These properties are connected to reorganization at a mesoscopic level related with the apparition of at least two distinct phases:

crystalline grains of a few nanometers embedded in strongly disordered grain boundaries. The determination of grain sizes, their statistical distribution and the proportions of grains and grain boundaries can be obtained by conventional powder diffraction (XRD) and transmission electron microscopy (TEM). An access to the local structure, i.e. the geometric and electronic properties of the constituting ions or paramagnetic impurities and their local coordination spheres can be achieved only with the help of local probe spectroscopic methods like electron paramagnetic resonance (EPR) (for paramagnetic centres), Mössbauer spectrometry and nuclear magnetic resonance (NMR). In the last five years, the two latter [1–3] have shown their efficiency in the field of nanostructured fluorides. Furthermore, since in general both paramagnetic defects and transition metal ions incorporated in diamagnetic hosts may lead to local activation of the matrix, it is of basic interest to study their local properties and their changes caused by mechanical and thermal treatments of the matrix.

In this study a corundum powder (α-Al_2O_3) was used as a model system to monitor the effect of mechanical ball milling. Corundum was chosen because it plays a crucial role in catalysis and material science. Moreover, it offers the opportunity to study the local structure of both the 'matrix' aluminium sites by ^{27}Al-MAS-NMR and the Al substituted Fe^{3+} site by EPR spectroscopy. These techniques are worked out because they can provide valuable structural information due to their ability to discriminate between resonating species with different atomic environments. Actually, Fe^{3+} fine structure and ^{27}Al quadrupolar parameters are expected to be sensitive to the effect of mechanical milling [4, 5].

Starting from crystalline powders and going to partially ordered and finally to nanostructured corundum powders as prepared by milling, it is the aim of the present study:

(i) to get a consistent interpretation of both the complex Fe^{3+}-EPR spectra and the ^{27}Al-MAS-NMR spectra and to establish relations between the spectroscopic parameters of both ions, and
(ii) to deduce relations between the local structure seen by ^{27}Al nuclei and Fe^{3+} ions and the structural characteristics of the matrices as found by XRD and TEM measurements.

This study touches some of the unanswered questions in the field of corundum powders in relation with preparation processes. It implies the assignment of the spectra and quantitative determination of the zero-field splitting (ZFS) (Fe^{3+}) and quadrupolar (Al^{3+}) parameters for each step of matrix disorder.

2. Experimental details

Material. The corundum powder (α-Al_2O_3, 99.99%, Aldrich Chem. Comp., Inc) was milled in a commercial planetary ball mill (Fritsch Pulverisette 7). Four agate balls were used in each agate vial (m_{balls}: 16.5 g; m_{sample}: 1.0 g). The agate material was chosen to allow a discrimination between the corundum material and a probable contamination by the vial. The milling intensity $I = 6$ corresponds to a vial rotation speed of 800 rotations min^{-1}. The milling time was varied from 5 min to 60 h. Fe^{3+} ions, allowing EPR spectroscopic measurements, are present in the commercial α-Al_2O_3 as impurities at a level of about 2 ppm.

XRD. Mean grain sizes and amorphous parts in the matrices were determined by XRD analysis using the equipment HZG-4C in the two theta range from 4° to 64° (Präzisionsmechanik Freiberg, Germany; radiation: Cu Kα; step scan: 0.02°, step time: 5 s). For the determination of the amorphous part the samples were mixed with an internal standard of a known degree of crystallinity (silicon, mean grain size: ∼230 nm, mixed mass ratio 1:1).

Following that, the program BGMN [6][4] was used to extract finally the amorphous content and to estimate the mean size of the corundum crystallites. For that estimation a simple isotropic approximation was applied by the program. High-resolution XRD patterns for the unmilled and 60 h milled samples at room temperature were recorded using a Bruker D8 diffractometer (Cu Kα radiation) in the two theta range from 16° to 136° (step scan: 0.02°, step time: 14.4 s).

A Rietveld-refinement of the high-resolution XRD patterns for the unmilled and the 60 h milled samples at room temperature was performed by using the FULLPROF program [7]. From the starting material the instrumental function (modified Thomson–Cox–Hastings pseudo-Voigt function) was determined and applied to refine the isotropic size parameter of the 60 h milled sample. The amorphous part was handled by introducing a second phase with the same crystallographic parameters but with different half-width parameters. Both methods (FULLPROF and BGMN-programs) extracted the structural data by taking into account only Bragg reflections connected with the analysis of the full diffraction profile.

TEM. The electron microscopy study was performed with a 200 kV JEOL 2010 electron microscope (tilt ±30°) fitted with a eucentric goniometer (60°) and equipped with an EDX analyser. A few droplets of a suspension of powder in alcohol were deposited on a carbon-coated holey film.

NMR. The ^{27}Al ($I = 5/2$) NMR spectra were recorded on a Bruker Avance 300 spectrometer corresponding to a ^{27}Al resonance frequency of 78.2 MHz. MAS experiments were realized with a high speed probe using 2.5 mm zirconia rotor. The radio-frequency magnetic field strength (in frequency unit) was set to 62.5 kHz resulting in $t_{\pi/2} = 4$ μs for a solution of $Al(NO_3)_3$. The excitation pulse duration was chosen equal to 1 μs which is slightly outside the linear irradiation regime minimizing distortion of the spectra [8]. It was carefully checked that this longer pulse length does not affect the spectra but results in a better signal to noise ratio.

The recycling delay between each acquisition was fixed to 5 s. 32 K data sampling points were recorded over a 2 MHz spectrum width. Processing of the free induction decay was realised using Bruker XWINNMR software. The first 60 points corrupted by electronic interferences were removed and 86 points were reconstructed by linear prediction. 1 M solution of $Al(NO_3)_3$ was used as a reference for ^{27}Al chemical shift. On all the figures the origin of the frequency scale (0 kHz) always corresponds to 0 ppm.

SATRAS NMR (satellite transition NMR) spectra were recorded. It requires an accurate setting of the magic angle which was obtained by minimization of the line width of the sidebands of the satellite transitions of ^{23}Na in $NaNO_3$ powder.

The measured parameters are the quadrupolar frequency $\nu_Q = 3eQV_{ZZ}/2I(2I-1)h$ and the asymmetry parameter $\eta_Q = (V_{XX} - V_{YY})/V_{ZZ}$, where Q is the quadrupolar moment, V_{XX}, V_{YY}, V_{ZZ} are the principal components of the electric field gradient tensor, with the condition $|V_{ZZ}| \geqslant |V_{YY}| \geqslant |V_{XX}|$ leading to $0 \leqslant \eta_Q \leqslant 1$. The isotropic chemical shift δ_{iso} used for the spectrum simulation is defined as $\delta_{iso} = \frac{1}{3}(\delta_{XX} + \delta_{YY} + \delta_{ZZ})$: $\delta_{ii} = \sigma_{ref} - \sigma_{ii}$ where $\sigma_{ii}(i = x, y, z)$ are the principal components of the shielding tensor.

EPR. For the X-band ESR measurements both the spectrometer ER 100D (Bruker, Germany) and the ERS 300 (ZWG, Berlin-Adlershof, Germany) were used. Low-temperature measurements (4.2 K) were performed with a flow-cryostat Heli-Tran (APD Cryogenics, USA).

[4] Program BGMN: a program for quantitative phase analysis using a new Rietveld-algorithm assisted by improved stability and convergence behaviour.

For Q-band measurements the microwave bridge ER051QG and the cavity ER5106QT (Bruker, Germany) were adapted to the ERS 300 spectrometer.

The Fe^{3+} EPR was interpreted on the basis of a spin-Hamiltonian, which has the general form [9]:

$$\hat{H} = \beta \cdot \vec{B}_0 \cdot g \cdot \vec{S} + \sum_{n,m} B_n^m \cdot O_n^m$$

where O_n^m is a spin operator ($n = 2, 4$; $-n \leqslant m \leqslant +n$).

The ZFS-parameters of the Fe^{3+} ions were determined using the simulation program ESR-MAKRO-1 [10] which is based on the complete diagonalization of the spin-Hamiltonian matrix and takes into account statistical distributions of the ZFS parameters of second and fourth order[5] (b_2^m, b_4^m) to represent the disorder in the sample.

3. Results

XRD. The relevant part of the x-ray powder diffractogram of the starting material α-Al_2O_3 is given in figure 1(*a*). Figure 1(*b*) shows the behaviour of two essential reflections of corundum in dependence on milling time. Obviously the mechanical treatment results in a broadening of the diffraction peaks and a decrease of their amplitudes. Using the BGMN program [6], this effect is related to the grain size of the crystallites which decreases and to the amorphous content which increases. Starting from about 350 nm (unmilled sample) the mean grain size of Al_2O_3 is reduced to 13 nm after 60 h of milling. Figure 2 depicts the changes of grain sizes in dependence on milling time. It turns out that the grain size is reduced to about 1/10 of the starting value after 2 h of milling. According to the refinement results, the amorphous amount in the samples evolves from 20% after 5 min milling to ∼40% after 60 h which appears as a maximum value from the BGMN calculations [6] (see also figure 8). In order to check a possible occurrence of so far unresolved additional phases, high-resolution XRD was performed for the 60 h milled sample as well as for comparison for the unmilled one. The corresponding diffractograms are compared in figure 1(*c*). In addition to what is observed in the low-resolution XRD measurements a very broad contribution shifts the diagram towards higher values for the 60 h milled sample. The x-ray data for the two samples (unmilled and 60 h milled sample) are collected in table A.1 in the appendix. They give evidence for a nanocrystalline phase (grain size ∼13 nm) and a pseudo-amorphous phase where the long range order is lost. Finally, SiO_2, which was also found in the 60 h milled sample was taken into account for the Rietveld analysis by using the pattern matching mode of FULLPROF [7]. Changes of the lattice constants and atomic positions obtained for the 60 h milled sample are given in tables 1 and A.1. While the cell constant c increases by 0.1%, the increase of the cell parameter a amounts only 0.01%.

TEM. TEM examinations were performed to observe the differences of sizes and shapes of the grains due to the milling procedure. Whereas the grains of α-Al_2O_3 show an elliptic, in part hexagonal shape (figure 3(*a*)), the large mechanical impact leads to more spherical grains of very small diameter (figure 3(*b*)). Several different micrographs were used to perform evaluations of grain size distributions for the unmilled and 60 h milled samples. About 40 particles present on each photo were counted and their diameters could be measured with an error of ±4 nm. The mean values of the grain size distributions (unmilled sample: ∼300 nm width, ∼450 nm length; 60 h milled sample: ∼17 nm) correspond well to those determined by XRD measurements.

[5] The well known relations as given in [11] are used for the transformation between b_n^m and B_n^m.

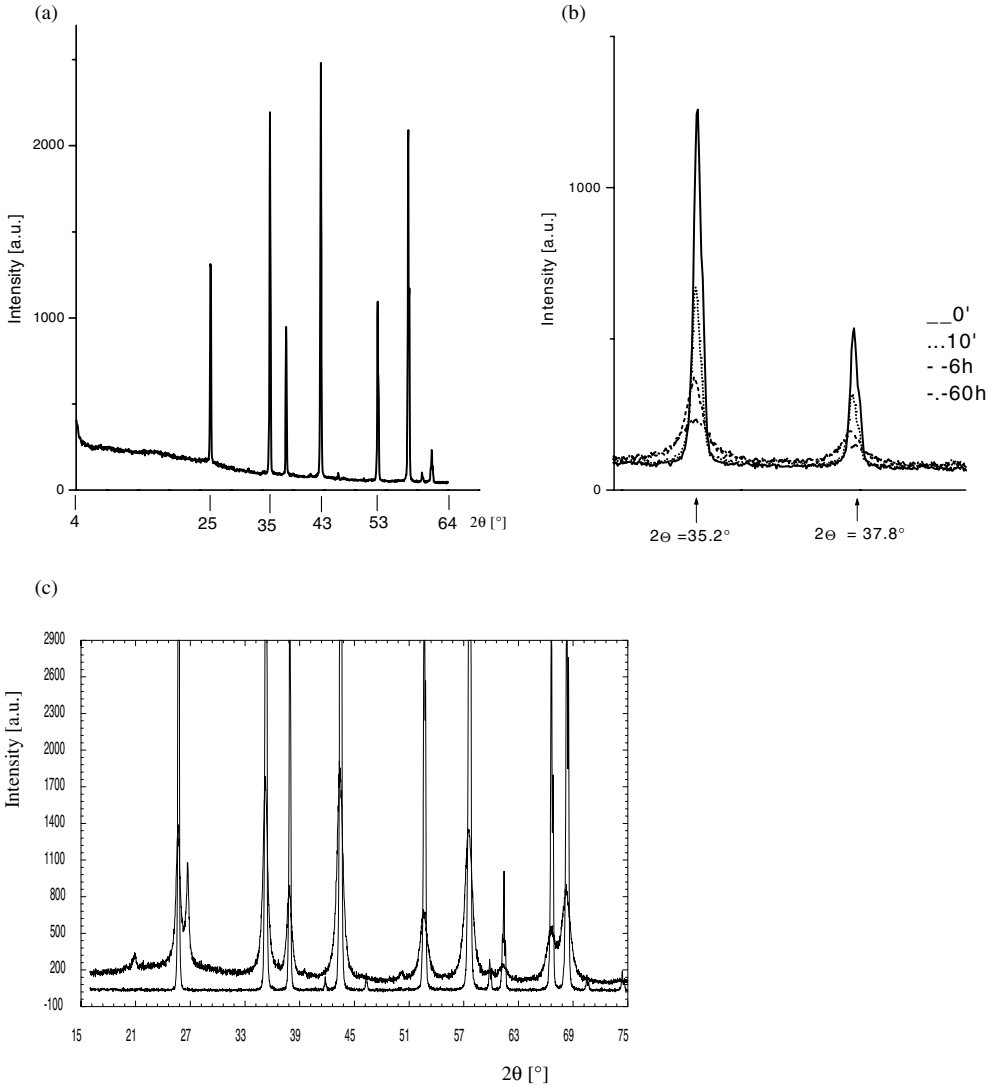

Figure 1. X-ray powder diffractograms of, (*a*) unmilled α-Al_2O_3 (low-resolution), (*b*) selected reflections of α-Al_2O_3 in dependence on milling time (low-resolution), (*c*) unmilled and 60 h milled samples (high-resolution).

Table 1. Atomic positions and cell parameters of unmilled and 60 h milled corundum samples obtained by high-resolution x-ray measurements (cf table A.1).

Milling time	Atom	x	y	z
0	Al	0	0	0.352 19(5)
	O	0.307 0(2)	0	1/4
60 h	Al	0	0	0.352 2(1)
	O	0.309 4(5)	0	1/4
		a(Å)		c(Å)
0		4.760 84(3)		12.996 38(8)
60 h		4.761 2(2)		13.011 8(8)

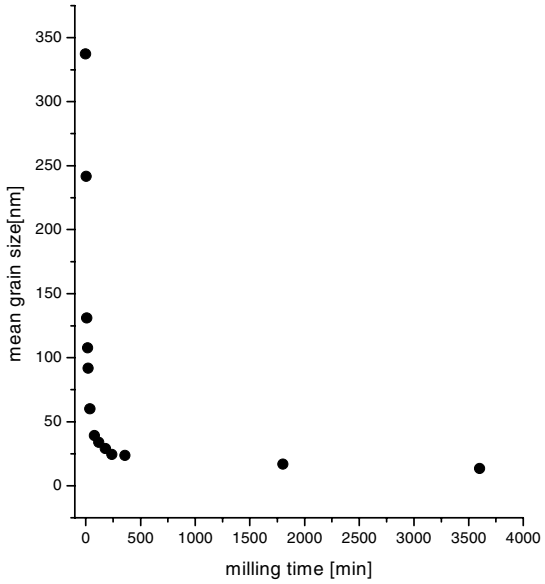

Figure 2. Dependence of the mean grain size of milled corundum samples on the milling time.

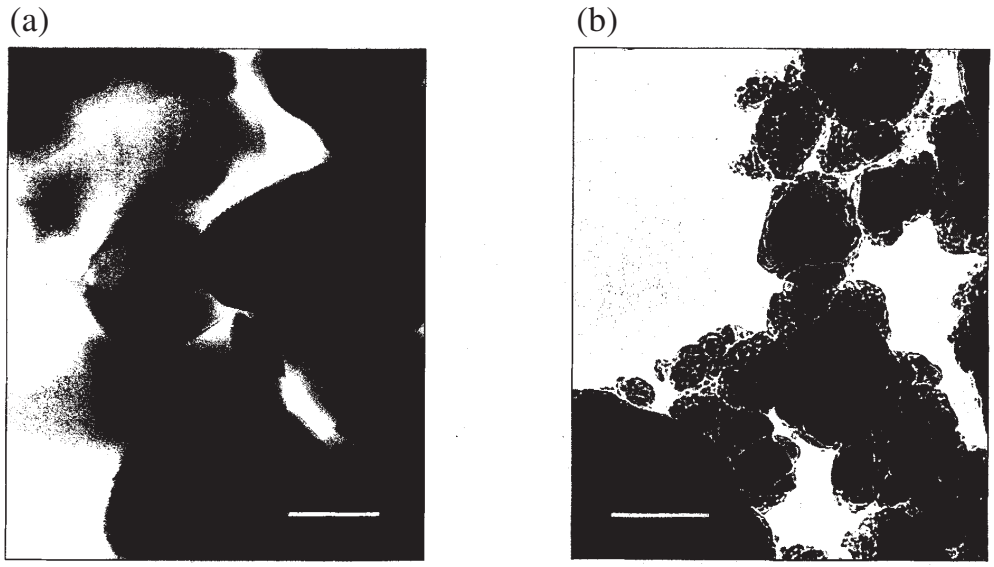

Figure 3. Transmission electron micrographs of the crystalline parts of: (*a*) unmilled α-Al_2O_3, (*b*) Al_2O_3 milled for 60 h; scale: 200 nm.

NMR. SATRAS NMR experiments were performed as previously applied to oxide glasses by Jäger *et al* [5]. It has been proved to be a useful technique in determining the interaction parameters of quadrupolar spin systems (spin $I > 1/2$) especially when the quadrupolar frequency is 'small' i.e. when the particular structure of the central transition (CT) $1/2 \leftrightarrow -1/2$ due to second order effects is not resolved [12]. This is nearly the case in pure Al_2O_3 (figure 4, inset).

As shown by Skibsted [13], despite the poor resolution of the CT line, reliable information can be obtained through the NMR satellite transitions. When pulse duration effects can

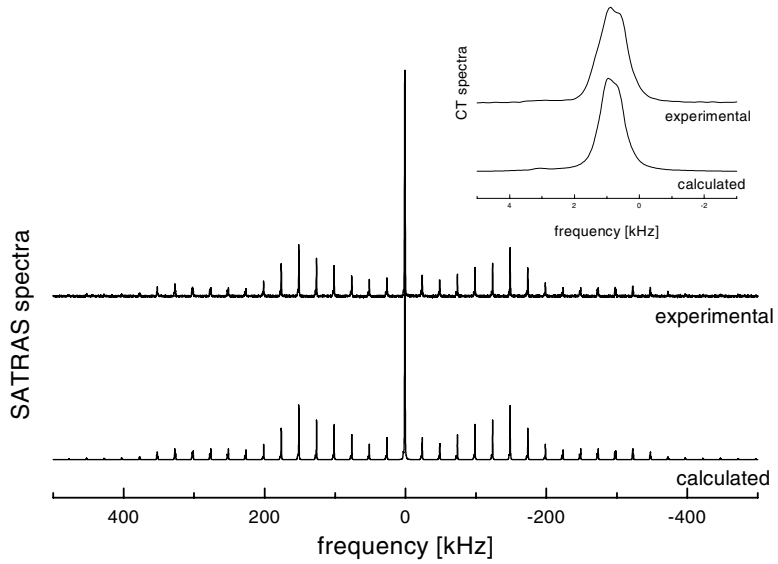

Figure 4. Experimental and calculated SATRAS NMR spectra of ^{27}Al in the crystalline α-Al_2O_3. Inset: central transition.

be neglected and when the chemical shift interaction is much smaller than the quadrupolar interaction, the SATRAS spectrum is symmetric. The quadrupolar frequency ν_Q roughly determines the extent of the NMR spectrum and the asymmetry parameter η_Q the shape of the envelope of the sidebands. In the starting corundum the ^{27}Al NMR spectrum measured at a spinning speed of 25 kHz is spread symmetrically over 400 kHz on each side of the CT line (figure 4).

The theoretical treatment of SATRAS NMR spectra was previously developed [13] and a few errors in the original expressions were corrected recently [14]. As a misprint occurred in this later paper, the correct formula giving the second order frequency shift ν_c of the spinning side bands due to the quadrupolar interaction for the $m \rightarrow m-1$ transition is given below:

$$\nu_c = \frac{1}{2\nu_L}\left[\frac{C_Q}{4I(2I-1)}\right]^2 (C^{(1)}[4I(I+1) - 24m(m-1) - 9] + C^{(2)}[2I(I+1) - 6m(m-1) - 3])$$

where ν_L is the Larmor frequency and C_Q is related to the quadrupolar frequency according to: $C_Q = \frac{2I(2I-1)}{3}\nu_Q$.

The expressions of $C^{(1)}$ and $C^{(2)}$ are given in [13].

In crystalline α-Al_2O_3, the spectrum simulation takes into account this second order frequency shift and allows to determine the CT line position at 8 ppm the quadrupolar frequency equal to 357 kHz, the asymmetry parameter $\eta_Q = 0$ and $\delta_{iso} = 16$ ppm as previously obtained by Skibsted *et al* [13]. The calculated spectrum is compared with the experimental one on figure 4. The fine agreement supports the simulation procedure.

SATRAS spectra measured at a spinning rate of 25 kHz for samples with milling time ranging between 5 min and 60 h are presented in figure 5 together with the spectrum of unmilled corundum. First, as no extra central line appears which could be characteristic of 4- or 5-fold coordinated Al^{3+} ions, it can be concluded that the aluminium ions remain in a 6-fold oxygen coordination. Second, the main changes of the NMR spectra are a progressive smoothing of

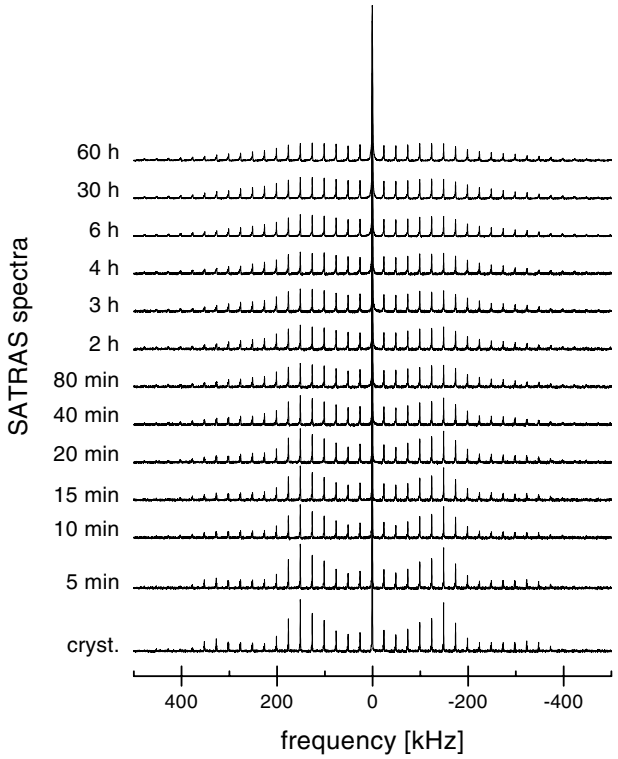

Figure 5. Dependence of the NMR SATRAS spectra of ^{27}Al in corundum on the milling time.

the envelope of the spinning sidebands, an increasing broadening of both central and satellite transitions (figure 6) and the appearance of a slight asymmetry of the lines on the right side for the CT and on the left one for the satellites. These features are characteristic of a distribution of Al environments.

As previously demonstrated for GaF_3 [3], in such mechanically milled powders, two contributions called grains and grain boundaries are expected: the grain structure is close to the structure of the starting material (here α-Al_2O_3), whereas the grain boundary structure is close to that of an amorphous phase. The NMR spectra related to this amorphous phase may be reconstructed using a so called Czjzek distribution [15] of the quadrupolar parameters:

$$P(\nu_Q, \eta_Q) = \frac{1}{\sqrt{2\pi}\sigma^d}\nu_Q^{d-1}\eta_Q(1-\eta_Q^2/9)\exp\left\{-\frac{\nu_Q^2(1+\eta_Q^2/3)}{2\sigma^2}\right\}$$

where σ and d are two adjustable parameters [16].

A successful reconstruction of the SATRAS spectra of corundum at different milling times was obtained by using a superimposition of the NMR crystalline spectrum with an amorphous one. Our computer program written in FORTRAN 90 was used to calculate the SATRAS NMR spectra assuming ideal sample irradiation. The parameters of the corresponding Czjzek distribution leading to the best fit were $\sigma = 350 \pm 50$ kHz and $d = 3$ (as usual for octahedral coordination). σ is determined by the spectral frequency width which is not affected by the milling treatment. This corresponds to a mean value of the quadrupolar frequency close to that of the unmilled sample. As the 6-fold coordination of the Al atoms is preserved, the δ_{iso} of the amorphous phase was assumed to be identical to that of the crystalline one. Figure 7 shows

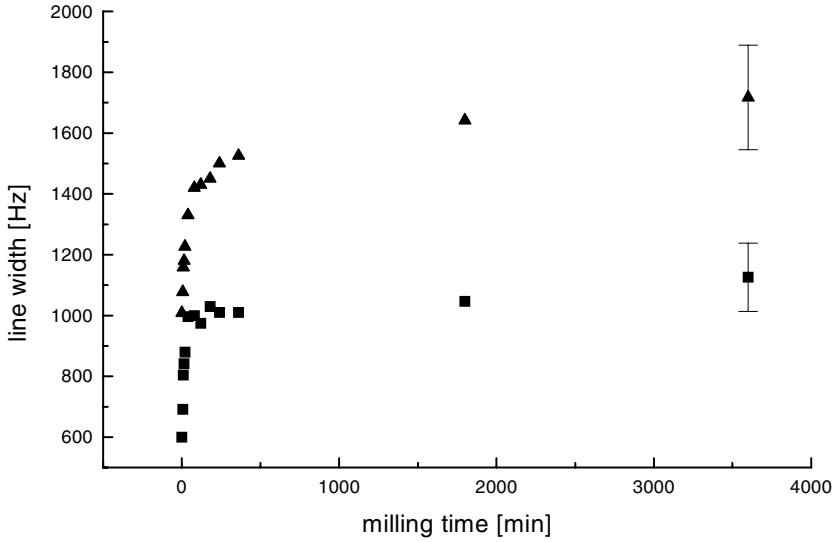

Figure 6. Evolution of the linewidths (Hz) of the central transition (CT) and of the $\pm 3/2 \leftrightarrow \pm 1/2$ transitions versus the milling time (the low signal to noise ratio of the $\pm 5/2 \leftrightarrow \pm 3/2$ sidebands prevents to do the same plot for these transitions). ■ $\pm 3/2 \leftrightarrow \pm 1/2$; ▲ CT.

the fine agreement between experimental and calculated spectra for the 60 h milled sample which exhibits the line asymmetry experimentally observed. From the integrated intensities of the calculated spectra, the ratios of the crystalline and amorphous phases were determined as a function of the milling time. The amorphous ratio is plotted versus the milling time in figure 8. It may be noticed that these variations are similar to those of the linewidths of the CT and $\pm 3/2 \rightarrow \pm 1/2$ transition lines plotted in figure 6.

EPR. Whereas the corundum matrix exhibits a decrease of the mean grain size and an increase of the amorphous part by milling, it is interesting to study how the paramagnetic Fe^{3+} impurity environment is influenced by mechanical perturbations of this hard material. Indeed, this local point defect may induce specific environment alteration, different from that observed for Al nuclei.

Figure 9 shows experimental X-band (9.3 GHz) EPR spectra of the unmilled α-Al_2O_3 and milled samples for different milling times measured at room temperature and 4.2 K. At least, four distinct paramagnetic species are evidenced:

(i) The x-band signals at effective g-values $g' \sim 13$, $g' \sim 5.2$, $g' \sim 2.0$ are characteristic of isolated Fe^{3+} ions in crystalline corundum powder [17]. Their intensities[6] decrease very fast with increasing milling time. It is difficult to observe these signals after a milling time of 2 h. Although corundum is a very hard material, the x-band ESR spectra of Fe^{3+} ions give evidence for pronounced changes even for short milling times of 5–20 min.

(ii) After 5 min milling, an intense and broad signal appears in the $g' \sim 2$–3 region at 298 K. It is enhanced and shifted to lower g'-values with increasing milling time up to 20 min. It is interesting to note that this signal is not observed at 4.2 K. It indicates the formation of paramagnetic Fe (III)-clusters, which become antiferromagnetically coupled units at low temperatures.

[6] The intensity used here corresponds to the relative intensity in the spectrum, and not to the absolute intensity obtained after integration.

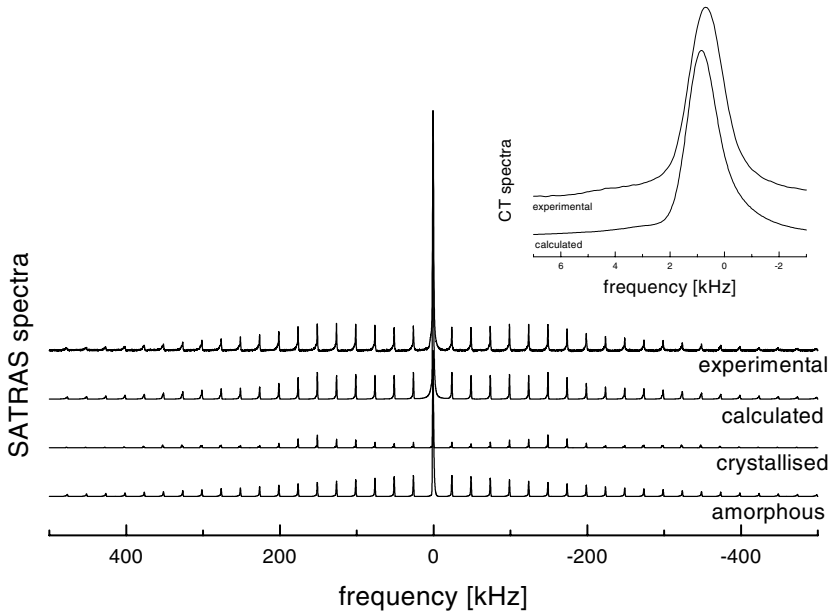

Figure 7. Experimental and calculated SATRAS NMR spectra of ^{27}Al in the 60 h milled corundum powder. Inset: experimental and calculated central transition; the calculated spectrum is a sum of 80% of the amorphous and 20% of the crystalline spectrum.

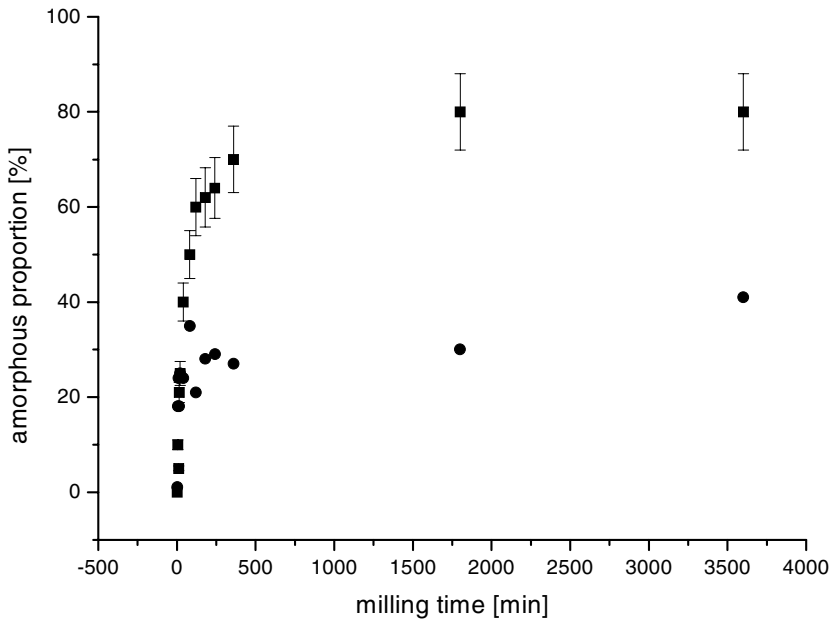

Figure 8. Amorphous proportion in dependence on milling time determined by NMR (■) and XRD (●).

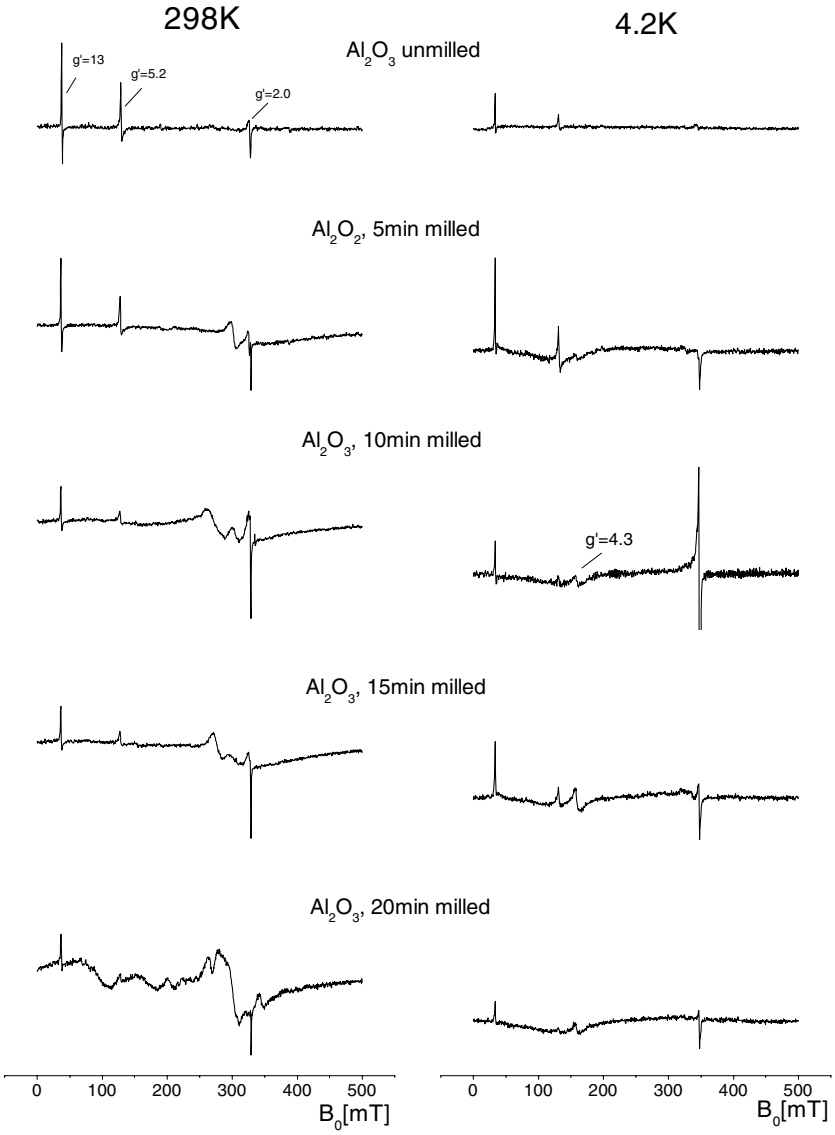

Figure 9. X-band ESR spectra of milled Al_2O_3 samples taken at 298 K and 4.2 K ($B_1 \perp B_0$) detection.

(iii) An additional resonance transition at $g' = 4.3$ becomes observable at 4.2 K already after 5 min milling. This transition enhances dramatically and, finally dominates the ESR response in X-band at 4.2 K starting with 2 h milling. It is the typical X-band signal of Fe^{3+} ions in amorphous and glassy oxide materials [18].

(iv) An additional narrow line centred at $g' \sim 2$ originates from a defect which is not related to Fe^{3+} but stabilized by the abrasive wear from the agate sample container and balls (SiO/h^+ centre [19]; as already mentioned, a certain amount of SiO_2 was detected in the samples by x-ray measurements). Note that the X-band spectra of the samples milled for 2 and 4 h show a remarkable intensity in the low-field region.

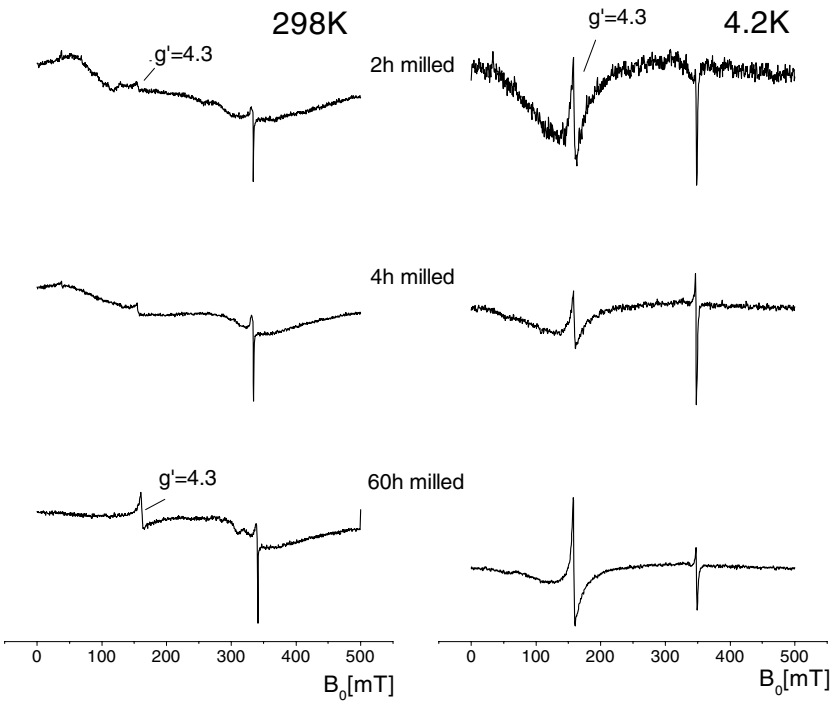

Figure 9. (Continued.)

In the following, the discussion is focused on a quantitative interpretation of the Fe^{3+} ion spectra in the crystalline and amorphous phases (paramagnetic species i and iii).

Fe^{3+} ions in crystalline phase (α-Al_2O_3). According to their local symmetry $\bar{3}$, the EPR spectra of $Fe^{3+}(S = 5/2)$ ions in crystalline corundum may be interpreted with the following spin-Hamiltonian:

$$H = \beta \cdot \vec{B}_0 \cdot g \cdot \vec{S} + \tfrac{1}{3} b_2^0 O_2^0 + \tfrac{1}{60}(b_4^0 O_4^0 + b_4^3 O_4^3)$$

where O_n^m are spin operators [9]. From the reconstruction of the spectrum at room temperature, the correct line positions are obtained with:

$$b_2^0 = 1683 \times 10^{-4}\,\mathrm{cm}^{-1}, \qquad b_4^0 = -110 \times 10^{-4}\,\mathrm{cm}^{-1}, \qquad b_4^3 = 2181 \times 10^{-4}\,\mathrm{cm}^{-1}$$

in agreement with [20]. The constant line width of the $g' \sim 13$ line is directly connected with the constant value of the b_2^0. It means that the mechanical perturbation does not lead to a change of the axial b_2^0 value (cf figure 9). Nevertheless, in order to reproduce properly the line intensities and peak to peak line widths at $g' \sim 13$ and $g' \sim 5.2$ and based on the analysis given in [4, 20], a distribution of the b_2^2 ZFS-parameter with a mean value of zero has to be assumed. The amplitude ratio of the two main signals at $g' \sim 13$ and $g' \sim 5.2$ in X-band was calculated performing powder spectra calculations including Gaussian distributions of the ZFS-parameter b_2^2 [4, 10]. The result is given in figure 10, plotting the dependence of the ratio of the amplitudes $A_{(g'=13)}/A_{(g'=5.2)}$ versus the width of the Gaussian distribution function $2\Gamma_{b_2^2}$. The reconstruction of the Fe^{3+} X-band ESR spectrum of the unmilled powder succeeded with $2\Gamma_{b_2^2} = 35 \times 10^{-4}$ cm^{-1}, whereas 20 min milling enlarges the distribution width to $2\Gamma_{b_2^2} = 140 \times 10^{-4}$ cm^{-1}. The determination of this parameter was not possible

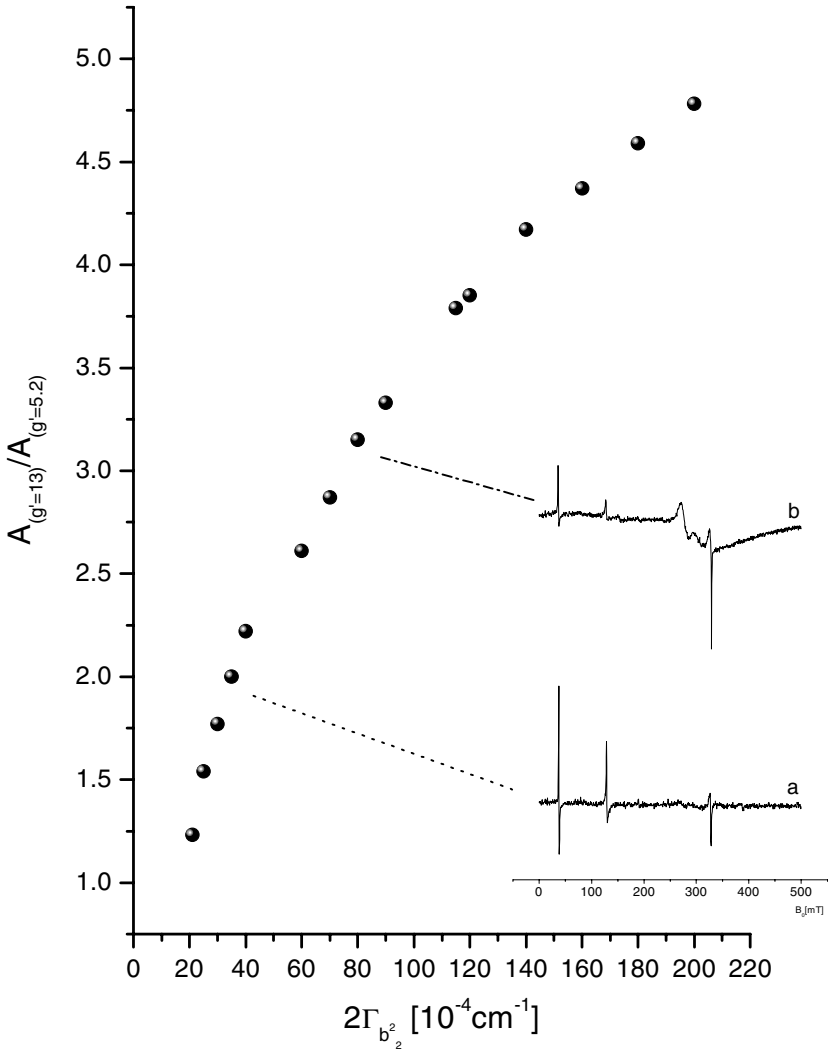

Figure 10. Dependence of the amplitude ratio $A_{(g'=13)}/A_{(g'=5.2)}$ of the two low-field corundum signals versus the width of the Gaussian distribution function of the ZFS parameter b_2^2; the calculation of each powder spectrum was performed with the parameters: $b_2^0 = 1683 \times 10^{-4}\,\mathrm{cm}^{-1}$, $b_4^0 = -110 \times 10^{-4}\,\mathrm{cm}^{-1}$, $b_4^3 = 2181 \times 10^{-4}\,\mathrm{cm}^{-1}$, $b_2^2 = 0$ as mean value, individual line width: 0.2 mT. Two experimental X-band spectra are given as inset: (*a*) unmilled α-Al_2O_3; (*b*) Al_2O_3, 15 min milled.

at larger milling times due to weak intensities of the signals. It is worth noticing that the ratio $\lambda = b_2^2/b_2^0$ is the local asymmetry parameter at the Fe^{3+} site which may be compared to the asymmetry parameter η_Q measured in the NMR experiments. EPR measurements and calculations lead to $2\Gamma_\lambda = 0.02$ for the unmilled corundum and $2\Gamma_\lambda = 0.08$ for the 20 min milled sample.

The description of the local environment of the Fe^{3+} ions may be achieved using the superposition model of Newman [21, 23, 24] which allows to relate the spin-Hamiltonian parameters of Fe^{3+} ions to the atomic positions of the Fe^{3+} nearest neighbours. The b_2^0 value of Fe^{3+} ions was calculated according to:

$$b_2^0 = \tfrac{3}{2} \cdot \bar{b}_2(R_1) \cdot (3\cos^2\theta_1 - 1) + \tfrac{3}{2} \cdot \bar{b}_2(R_2) \cdot (3\cos^2\theta_2 - 1)$$

with a deviation of only 3% from the experimental value. This result encouraged to use the $2\Gamma_{b_2^2}$-distribution width for a description of the influence of mechanical milling on the decrease of the local site symmetry as follows[7]:

$$b_2^2 = \tfrac{9}{2}\bar{b}_2(R_1) \cdot \sin^2\Theta_1 \cdot \sum_{i=1}^{3} \cos 2\Phi_i = \tfrac{9}{2}\bar{b}_2(R_2) \cdot \sin^2\Theta_2 \cdot \sum_{i=4}^{6} \cos 2\Phi_i$$

with $\Phi_1 = \varphi_1,\ \Phi_2 = \varphi_1 + \frac{2\pi}{3},\ \Phi_3 = \varphi_1 + \frac{4\pi}{3}$ and $\Phi_4 = \varphi_2,\ \Phi_5 = \varphi_2 + \frac{2\pi}{3},\ \Phi_6 = \varphi_2 + \frac{4\pi}{3}$.

In this context Φ_i are the angles between the projections of two kinds of Fe–O bonds ((Fe–O_1) and (Fe–O_2)) onto the x–y plane and the x axis. In our case φ_1 equals 0°, and φ_2 equals 56.8°. Whatever the values of φ_1 and φ_2 are, b_2^2 equals zero. Among different possibilities, th decrease of the local site symmetry may be explained by the $\Delta\varphi$ distribution of one of the six values of Φ_i around its value in the trigonal phase. If we consider the variation of Φ_4, we receive:

$$2\Gamma_{b_2^2} = |\tfrac{9}{2} \cdot \bar{b}_2(R_2) \cdot \sin^2\Theta_2 \cdot 2\sin(2\varphi_2) \cdot \Delta\varphi|$$

Whereas even in the unmilled corundum sample the small $2\Gamma_{b_2^2}$ distribution of 35×10^{-4} cm^{-1} leads to a $\Delta\varphi$-value of 0.04° compared to an ideal powder ($2\Gamma_{b_2^2} = 0$) as a consequence of the incorporated Fe^{3+} ions, the impact of 20 min milling enlarges the rhombic distortion up to $\Delta\varphi = 0.12°$ compared to the unmilled sample.

It reflects the changes of the local {∠OFeO}-bond angles and influences mainly the resonance transitions at $g' \sim 5.2$ (x-band). It represents an increase of the angular distribution as consequence of the increasing mechanical impact. This is in agreement with the idea of bond angles as more sensitive structural parameters than bond distances.

Fe^{3+} ions in amorphous parts. Following the evolution of the x-band spectra with increasing milling time, one can conclude that the local environment of the Fe^{3+} ions is transformed from the crystalline to the amorphous part. This indicates that Fe^{3+} ions are mainly found in the grain boundaries at the end of the milling process. It could mirror that Fe^{3+} ions are centres initiating the grain breaking and thus 'move' from the bulk to the grain boundaries.

It was previously demonstrated that calculations of the related EPR signals can only be achieved by a two-dimensional distribution of ZFS-parameters $\{b_2^0, b_2^2\}$ [10,26–28] or $\{b_2^0, b_4^0\}$, which are named {D, a} in [10]. From these calculations, as the line intensity at $g' \sim 4.3$ dominates the x-band spectrum at high milling times, a mean b_2^0 value much larger than $\sim 3300 \times 10^{-4}$ cm^{-1} (which corresponds to x-band quantum energy) together with $\lambda = \frac{b_2^2}{b_2^0}$ values distributed over the 0–1 range have to be assumed. This assumption is supported by the corresponding Q-band spectrum [29], since the integral intensity is rather small in the $g' \sim 2$ region compared to Fe^{3+} ions in oxide glasses [10, 18]. Then, the mean b_2^0 parameter which mirrors the axial symmetry of the Fe^{3+} site in the amorphous phase is at least about two times larger than in the crystalline one.

4. Discussion

XRD, NMR and EPR experimental results demonstrate the appearance of some amorphous phase in the milled samples with the shortest milling time. Together with the findings of

[7] Al–O distances: $R_1 = 1.966$ Å, $R_2 = 1.857$ Å; ∠(Al, O, c-axis): $\theta_1 = 47.7°, \theta_2 = 63.1°$ [25]; $\bar{b}_2(R_1) = -0.505\,68$ cm^{-1}, $\bar{b}_2(R_2) = -0.768\,56$ cm^{-1}, calculated according to Boizot [22] with a mean Fe–O distance of 2.019 Å.

TEM, they show that the mechanical treatment results in developing this amorphous phase and simultaneously reducing the crystalline one. However, whereas both XRD and NMR techniques indicate that even for the longest milling time the sample contains both crystalline and amorphous phases, EPR data are in favour of the presence of the Fe^{3+} ions exclusively in the amorphous phase for milling times larger than 20 h.

XRD and NMR results allowed to determine the relative proportions of amorphous and crystalline phases in the milled samples and their evolution with the milling time. Nevertheless, it appears a clear discrepancy between the two sets of measurements. The NMR determination gives a larger amorphous proportion. Such a result was already pointed out in nanostructured GaF_3 [30]. It can be explained in the following way: $\{AlO_6\}$-octahedra located in the periphery of the grains are expected to have distortions of the same order of magnitude as in the grain boundaries. XRD results may not be so affected by these distortions, whereas NMR includes this peripheral layer in the distribution of quadrupolar parameters attributed to grain boundaries. The difference may be properly accounted by one distorted peripheral layer of $\{AlO_6\}$-units.

The XRD procedure integrates even the outer tails of the Bragg peaks for the determination the crystalline proportions, which may lead to an underestimation of the amorphous part. A not negligible part of the intensity of the amorphous part can therewith be covered by the background.

Informative comparison can be made between NMR and EPR determination of the local distortion of the oxygen octahedra. Firstly, the greater sensitivity of EPR determines the effect of the mechanical treatment on the grains in terms of a slight rhombic deformation of the octahedra related to angle variation in the plane perpendicular to the axial distortion. It was checked that even the largest rhombic distortion observed here which should be $\eta_Q = 0.08$ does not significantly affect the NMR spectrum of the crystalline phase. Secondly, quadrupolar parameter distributions $\{\nu_Q, \eta_Q\}$ and $\{b_2^0, \lambda\}$, deduced from NMR and EPR respectively for the amorphous part, behave quite differently. In NMR, the mean quadrupolar frequency deduced from the Czjzek distribution is nearly equal to the quadrupolar frequency measured in the crystalline powder. This favours a grain boundary structure which keeps the fingerprints of the starting crystalline material. This result is opposite to that observed in more ionic nanostructured fluorides. The broad distributions of the η_Q and λ values are similar. In contrast, as previously outlined, the ratio of the mean b_2^0 value for Fe^{3+} in the amorphous phase to the b_2^0 value in the crystalline material is at least equal to two. This gives evidence for a stronger alteration of the Fe^{3+} ion environment than that of the Al^{3+} ion. This result can be interpreted in the following way: the Fe^{3+} ions represent a local perturbation. The mechanical energy is preferentially transferred from the matrix to the neighbourhood of this point defect resulting in a local activation of the matrix. These changes induced by the mechanical treatment can only be observed by Fe^{3+}-EPR spectroscopy.

5. Conclusions

Different complementary techniques were successfully applied to corundum nanostructured powders obtained by high-energy ball milling. Appropriate fitting procedures were used independently to analyse the experimental results. These results suggest that the milled powders consist of nanocrystalline grains embedded in amorphous grain boundaries even for the longest milling time. The grains can be described in terms of ordered $\{AlO_6\}$-octahedra as in the starting crystalline material, but exhibiting a slight rhombic distortion. The grain boundaries look like random arrangements of these octahedral units.

Local structural orders have been obtained through the applications of NMR and EPR spectroscopies. The local structure was determined by quadrupolar and ZFS parameter

distributions. The specific behaviour of the environment of the Fe^{3+} paramagnetic probe points out that such a point defect acts as an activation centre of the amorphisation process.

Acknowledgments

This work is partially supported by a PROCOPE program. We would like to thank J M Grenèche for a careful reading of the manuscript and constructive comments.

Appendix

Table A.1. Conditions of x-ray data collection and crystallographic characteristics of Al_2O_3 (in bold for the 60 h milled). R_p and R_{wp} are conventional Rietveld values, calculated after background subtraction.

Diffractometer	Bruker D8
Radiation	Cu Kα, graphite diffracted beam monochromator 38 kV, 28 mA
Divergence, antiscattering slits	0.5°, 0.5°
Receiving slit (°)	0.2
Angular range (°2θ)	16–136
Step scan increment (°2θ)	0.02
Count time (sec/step)	14.4
Miscellaneous	Room temperature, no sample rotation
Space group	$R\bar{3}c$ (No 167)
Cell parameters (Å)	$a = 4.760\,84(3)$, $c = 12.996\,38(8)$
	$\boldsymbol{a = 4.7612(2)}$, $\boldsymbol{c = 13.0118(8)}$
Volume / Z	255.106(2) Å$^3/Z = 6$
	255.44(2)
Number of reflections	59
Number of refined parameters	16
	12
Halfwidth parameters	$U = -0.0029(7)$, $V = 0.006(2)$, $W = 0.0172(6)$
Peak shape, X, Y	Thompson–Cox–Hastings pseudo-Voigt, 0.045(3), 0.013(1)
Zero point (°2θ)	0.105(2)
	0.099(4)
Asymmetry parameters	$P1 = -0.04(1)$, $P2 = 0.090(3)$
	$\boldsymbol{P1 = -0.008(9)}$, $\boldsymbol{P2 = -0.011(3)}$
Preferred orientation	[1 1 3] direction, 0.968(4)
	[1 1 3] $\boldsymbol{direction}$, **0.884(5)**
Reliability factors	$R_p = 0.132$, $R_{wp} = 0.168$, $R_{Bragg} = 0.058$, $\chi^2 = 4.77$
	$\boldsymbol{R_p = 0.874}$, $\boldsymbol{R_{wp} = 11.3}$, $\boldsymbol{R_{Bragg} = 0.057}$, $\boldsymbol{\chi^2 = 2.61}$
$\boldsymbol{Isotropic\ size\ (nm)}$	**12.4(3)**
$\boldsymbol{Crystalline,\ amorphous\ parts}$	**48%, 49%**
$\boldsymbol{SiO_2\ content}$	**3%**

References

[1] Guérault H and Grenèche J M 2000 *J. Phys.: Condens. Matter* **12** 4791
[2] Guérault H, Tamine M and Grenèche J M 2000 *J. Phys.: Condens. Matter* **12** 9497
[3] Bureau B, Guérault H, Silly G, Buzaré J Y and Grenèche J M 1999 *J. Phys.: Condens. Matter* **11** L423
[4] Klein J, Scholz G, Stösser R, Buzaré J Y and Silly G 2002 *J. Phys.: Condens. Matter* to be submitted
[5] Jäger C, Kunath C, Losso P and Scheler G 1993 *Solid State Nucl. Magn. Reson.* **2** 73
[6] Bergmann J, Kleeberg R, Taut T and Haase A 1997 *Adv. X-Ray Anal.* **40**

[7] Rodriguez-Carvajal J 2000 *Program FULLPROF 2k* Version 1.8a
[8] Smith M E and van Eck E R H 1999 *Prog. Nucl. Magn. Reson. Spectrosc.* **34** 159
[9] Abragam A and Bleaney B 1970 *Electron Paramagnetic Resonance of Transition Ions* (Oxford: Clarendon)
[10] Scholz G, Stösser R, Krossner M and Klein J 2001 *Appl. Magn. Reson.* **21** 105
[11] Jain V K and Lehmann G 1990 *Phys. Status Solidi* **159** 495
[12] Skibsted J, Vosegaard T, Bildsoe H and Jakobsen H J 1996 *J. Phys. Chem.* **100** 14 872
[13] Skibsted J, Nielsen N C, Bildsoe H and Jakobsen H J 1991 *J. Magn. Reson.* **95** 88
[14] Ding S and McDowell C A 2001 *Chem. Phys. Lett.* **333** 413
[15] Czjzek G, Fink J, Gotz F, Schmith H, Coey J M D, Rebouillat J P and Lienard A 1981 *Phys. Rev.* B **23** 2513
[16] Czjzek G 1982 *Phys. Rev.* B **25** 4908
[17] Stösser R and Scholz G 1998 *Appl. Magn. Reson.* **15** 449
[18] Stösser R and Nofz M 1994 *Glastech. Ber. Glass Sci. Technol.* **67** 156
[19] Stösser R, Nofz M, Momand J A, Scholz G and Sebastian S 1995 *Glastech. Ber. Glass Sci. Technol.* **68C1** 188
[20] Morin G and Bonnin D 1999 *J. Magn. Reson.* **136** 176
[21] Newman D J and Urban W 1975 *Adv. Phys.* **24** 793
[22] Boizot B 1996 *Thesis* Paris Université Pierre et Marie Curie
[23] Siegel E and Müller K A 1979 *Phys. Rev.* B **19** 109
Siegel E and Müller K A 1979 *Phys. Rev.* B **20** 3587
[24] Hemig M and Lehmann G *Superposition Model for the Zero-Field Splittings of 3d-ion EPR: Experimental Tests, Theoretical Calculations and Applications in Electron Magnetic Resonance of the Solid State* ed J A Weil (Ottawa)
[25] Zheng Wen-Chen 1998 *Physica* B **245** 119
[26] Yahiaoui E M, Berger R, Servant Y, Kliava J, Cugunov L and Mednis A 1994 *J. Phys.: Condens. Matter* **6** 9415
[27] Kliava J, Berger R, Servant Y, Yahiaoui E M, Cugunov L and Mednis A 1995 *Proc. 17th Int. Congress on Glass* vol 3 p 631
[28] Legein C, Buzaré J Y, Emery J and Jacoboni C 1995 *J. Phys.: Condens. Matter* **7** 3853
[29] Scholz G, Stösser R, Klein J, Buzaré J Y, Silly G and Ziemer B 2001 *Proc. 16eme Colloque Int. Optique-Hertzienne et Diélectriques* Le Mans
[30] Guérault H, Bureau B, Silly G, Buzaré J Y and Grenèche J M 2001 *J. Non-Cryst. Solids* **287** 65